BIO -SYNTHEIS OF Fe_2O_3@SiO_2@TiO_2-Ag NANOCOMPOSITE USING ORANGE LEAVES EXTRACT AND ITS APPLICATION IN THE DEGRADATION OF METRONIDAZOLE USING SOLAR PHOTOCATALYTIC METHOD

F. A. Haider **A. I. Alwared**
Researcher **Professor**
Dept. Envi. Col. Eng. University of Baghdad – Iraq
fatema.haider2011m@coeng.uobaghdad.edu.iq dr.abeer.wared@coeng.uobaghdad.edu.iq

ABSTRACT

Sol-gel, co-precipitation, and photo-deposition techniques were combined to create an effective method for making Fe_2O_3@SiO_2@TiO_2-Ag nanoparticles magnetically separable photocatalyst. FTIR, SEM, EDS, and XRD techniques were used to characterize the Ag-doped composite using FTIR, SEM, EDS, and XRD. In addition, the prepared composites' photocatalytic activity was investigated for the degradation of Metronidazole (MTZ). Approximately 96.85% of MTZ had decomposed after 2 hours of exposure to the sunlight with 20 mg/L of nanocomposite at a pH of 5, within 15 m/ L of MTZ. In addition, the outcomes showed that the 1-order kinetic model described the MTZ degradation kinetics. Furthermore, the results present that the Ag-doped composite was extremely efficient and reusable after 5 cycles of separation. Catching photo-generated electrons made charge separation easier by altering magnetic TiO_2 with silver nanoparticles, which led to an increase in the enhanced photoactive ability. These results, demonstrating the fabrication Fe_2O_3@SiO_2@TiO_2-Ag nanoparticles, hold promising applications for the elimination of pharmaceutical residues in the presence of sun exposure.

Keywords: MTZ antibiotic; advanced oxidation process; sunlight; orange peel; coreshell-Ag.

التخليق الحيوي لمركب نانوي Fe_2O_3@SiO_2@TiO_2-Ag باستخدام مستخلص أوراق البرتقال وتطبيقه في تحلل الميترونيدازول باستخدام طريقة التحفيز الضوئي الشمسي

فاطمة اكرم حيدر **عبير ابراهيم الورد**
باحث **استاذ**
قسم الهندسة البيئية– كلية الهندسة / العراق / جامعه بغداد

المستخلص

تم استخدام تقنيتي ال Sol–gel والترسيب المتعدد لتحضير محفز ضوئي نانوي باستخدام اوراق البرتقال Fe_2O_3 @ SiO_2 @ TiO_2– (Ag) القابل للفصل مغناطيسيًا ولقد تم توصيف خواص هذا المركب Ag–doped باستعمال تقنيات FTIR و SEM و EDS و XRD بالإضافة إلى ذلك كما تضمن البحث فحص نشاط التحفيز الضوئي باستعمال ضوء الشمس للمركب المحضر من أجل تحلل الميترونيدازول (MTZ)، وتوصل الباحث الى تحلل ما يقارب من 96.85 ٪ من MTZ بتركيز 15 ملغم /لتربعد ساعتين من التعرض لأشعة الشمس باستخدام 20 ملغم / لتر من المحفز الضوئي عند دالة حامضية 5 ، بالإضافة إلى ذلك تطابقت مع الموديل الحركي من الدرجة الأولى لوصف تحلل MTZ. علاوة على ذلك ، أظهرت النتائج أن مركب Ag–doped كان فعالًا للغاية ويمكن إعادة استخدامه بعد 5 دورات من الفصل. مما سبق اثبتت النتائج على كفاءة المركب المحضر بطريقة اقتصادية وبالاعتماد على مواد زراعية متوفرة وامنه على البيئة والتي تعد طريقة واعدة للتخلص من المخلفات الصيدلانية في وجود التعرض لأشعة الشمس.

الكلمات الافتتاحية: الميترونيدازول، الاكسدة المتقدمة، اشعة الشمس، اوراق البرتقال، الغلاف@النواة–الفضة .

Received: 27/02/2023, Accepted:17/05/2023, Published: August,2025

INTRODUCTION

Pharmaceutical compounds and personal care products, industrial chemicals, and herbicides are present in the aquatic environment, they are considered as emerging contaminants due to their potentially carcinogenic and mutagenic effect even at low concentrations. These contaminants can get into the environment through a variety of sources, including landfills, pharmaceutical manufacturing facilities, municipal wastewater, and industrial sewages. Pharmaceuticals and personal care items are developing toxins that environmental science communities and law enforcement organizations are very concerned about (1). Drinking water, groundwater, surface water, and sewage discharge have all had traces of antibiotics and other pharmaceuticals identified within them (19,31). Metronidazole (MTZ), or 2-methyl-5-nitroimidazole-1-ethanol, one of the most commonly used nitroimidazole antibiotics in the world, poses a serious threat to human life and health (21). This antibiotic is detected in treated wastewater and is characterized by its nonbiodegradability, high solubility in water, toxicity to aquatic systems, potential mutational properties, and carcinogenic properties. Since MTZ is extremely soluble in water and non-biodegradable, it can accumulate in aquatic environments, the tendency for mutagenicity, and carcinogenic potential, removing MTZ from water systems is a crucial concern (4,14). Adsorption, filtration, chemical oxidation, and biological processes are only a few of the technologies that have been used in recent years to remove various antibiotics. However, due to their resistance and low biodegradability qualities, biological approaches are unfavorable in the removal of antibiotics. Other systems, such as reverse osmosis and ion exchange, have some drawbacks, including challenging operation, expensive initial and ongoing expenditures, limited efficiency, and sludge formation (2). One of the advanced oxidation processes is heterogeneous photocatalysis, which relies on a semiconductor with a suitable energy gap absorbing photons directly or indirectly from UV or visible light (29). Furthermore, due to its environmental friendliness, high oxidation performance, and reduced energy and material consumption, heterogeneous photocatalysis is a possible substitute for the decontamination of antibiotics (14). The semiconductor for photocatalysis needs to be chemically or biologically inert, stable, affordable, simple to make, and generated without endangering people or the environment (29). Titania (TiO_2) has been shown to be the most appropriate among several oxide semiconductor photocatalysts for common environmental applications. TiO_2 is a potential material because it has high chemical and biological resistance, oxidizing power, low toxicity, and self-cleaning and antibacterial capabilities, but it has some drawbacks including the separation and recovery of nano-sized titanium-based photocatalyst are difficult and expensive in practice. High catalyst losses may result from using traditional separation techniques like centrifugation and filtration. Additionally, centrifugation consumes a significant amount of energy, which could result in secondary pollution. Thin TiO_2 films may be simpler to separate and restore, but because of the much reduced effective surface area, they have much lower photocatalytic activity. As a result, creating a multi-purpose photocatalytic system that is highly photoactive and economical to recycle is difficult (10). To solve these problems, the removal of nano-TiO_2 from aqueous suspensions, which is a significant problem, can be resolved by some researchers who have created granular TiO_2 with a magnetic core and photoactive shell. They demonstrated that the composite nanoparticles could be easily separated by the magnetic field as a result of their magnetic property (27). Unfortunately, photo-dissolution may also place, resulting in the separation of catalysts from the magnetic iron oxide core. This not only alters the characteristics of the magnetic iron oxides but also reduces the photocatalytic activity. The inert layer, such as SiO_2, serves as a barrier for both electrons and holes, limits any photoexcitation effects from the iron oxide, and keeps the iron oxide from scavenging excited carriers from the catalysts (18). Researchers have tried to create a TiO_2 visible-light antibacterial agent to address these issues. There are three common methods for getting such agents ready: (1) connecting TiO_2 with a small-band-gap semiconductor to

increase light absorption into the visible range (8); (2) doping TiO_2 with noble metal ions or transition metal ions such Pt, Au, Ag, V, Cr, Mn, Fe, Co, and Ni (27); (3) doping TiO_2 with nitrogen (28).Silver nanoparticles have been suggested as a viable choice for TiO_2 modification since they are very inexpensive when compared to other noble metals, exhibit bactericidal properties, and exhibit unique oxygen adsorption behavior. According to theory, electron transfer to TiO_2 caused by visible light absorption by silver surface plasmons leads to charge separation and visible light activation (11). In addition, the properties of synthesis TiO_2@Ag core-shell nanocomposite (CSNC) from Nigella Sativa were studied by (15). Several researchers have reported on the use of different magnetic composite microspheres for the purification of water such as Fe_3O_4-SiO_2-TiO_2 (46), $Fe_3O_4/SiO_2/TiO_2$,$Fe_3O_4/SiO_2/TiO_2/CeVO_4$ nanocomposites (30), and Fe_3O4-SnO_2-gC_3N4 (33). In this research, orange peels extract is used for the synthesis of Fe_2O_3@SiO_2@TiO_2–Ag NPs by the green route, and their characteristics are studied by SEM, XRD, FTIR, ultraviolet visible absorption spectroscopy, and BET analysis, then their photocatalytic ability for the degradation of MTZ under direct solar irradiation in a batch system was investigated.

MATERIALS AND METHODS

Chemical reagents: All of the compounds used in this investigation were analytical grade and used immediately in the experiments without being first purified; they were all purchased from Merck. Metronidazole ($C_6H_9N_3O_3$, molecular weight 171.2g/mol, water solubility 10mg/ml at 20 °C , pK_a of 2.55, Melting point 5.92×10^7 °C, K_H (5.92×10^7mol/dm^3.atm, and V_p of 4.07×10^{-7}Pa), was chosen as a target pollutant, its molecular structure was shown in Figure 1. Polyethylene glycol ($C_{2n}H_{4n+2}O_{n+1}$), silver nitrate $AgNO_3$, iron (III) chloride ($FeCl_3.6H_2O$, >99%), iron (II) chloride ($FeCl_2.4H_2O$), sodium hydroxide, hydrochloric acid, tetraethyl orthosilicate (TEOS, $SiC_8H_{20}O_4$), ethanol (ETOH, C_2H_5OH 95%), ammonium hydroxide (NH_4OH, 28%), titanium tetra isopropoxide TTIP (contained 95% anatase and 5% rutile).

Methodology of preparation

The process of Fe_2O_3@SiO_2@TiO_2-Ag nanocomposite fabrication was illustrated as follows:

Orange leaves: Fresh orange leaves were collected from Diyala farm East of Baghdad/ Iraq, were cleaned to remove dust and debris with distilled water, then dried in the sunlight for seven days, after that cutting the dried leaves fine pieces then grinded to get the finest powder. After that 20 g of dried leaves were mixed with 200 ml of deionized water for 30 minutes at 60 °C on a magnetic stirrer. Then after Whatman filter paper was used to filter the extract, which was then kept at 4° C for further use (30).

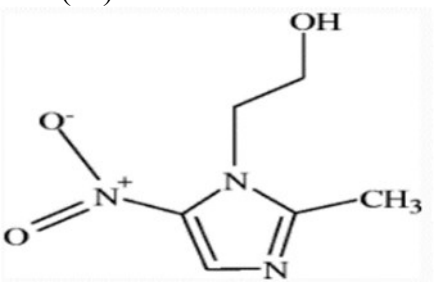

Fig.1. Molecular structure of MTZ

Fabrication of Fe_2O_3: Before adding the orange leaf extract, the $FeCl_3 \cdot 6H_2O$ and $FeCl_2 \cdot 4H_2O$ were first dissolved in 100 ml of distilled water at 80 °C in a 1:2 molar ratio. Next, 50 ml of the orange leaf extract was added to the iron chloride solution, and the entire mixture was then heated at 70 °C for 15 minutes while being continuously stirred with a magnetic stirrer until the pale yellow color turned brownish black. To achieve a final pH of 11, NaOH solution (3mol/L) was then added dropwise into the previously described solution while it was being constantly mechanically stirred for 30 min. The precipitate was agitated for 30 minutes at 80°C before cooling at room temperature. After the resultant particles were separated using a magnet, they were repeatedly washed with ethanol and deionized water until a pH of 7 was reached. The Fe_2O_3 nanoparticles were dried for eight hours at 60 °C in a vacuum (30).

Fabrication of Fe_2O_3@SiO_2

Iron oxide was combined with silicon dioxide by modifying the Stöber process with tetraethyl orthosilicate (TEOS) and Fe_2O_3 nanoparticles. An ultrasonic wave was used to disperse 1g of as-synthesized Fe_2O_3 in 20 ml

of water. Afterward, 4ml of aqueous ammonia solution (28% concentration) and 80ml of ethanol were added to the mixture. After that, 3 ml of TEOS was dropped dropwise into the mixed Fe2O3 nanoparticles under ultrasonic irradiation for 15 minutes. The precipitate was separated by an external magnetic and washed several times with water after stirring for half a day. As a final step, the collected precipitate was washed with water and dried at 60°C for 6 hours in a vacuum oven (17).

Fabrication of Fe_2O_3@SiO_2@TiO_2

In the preparation of Fe_3O_4@SiO_2@TiO_2, about 0.3 gm of the Fe_2O_3@SiO_2 was added to 15 ml of ethanol and the nanocomposite was mixed with a magnetic stirrer for ten minutes. After that, TTIP was added to the mixture with 20 ml of ethanol and put all of them into a magnetic stirrer for 90 minutes at 80 °C, and then all the mixtures were separated using external magnetic. Also, the nanoparticles were washed with ethanol and then deionized water several times and made dry in an oven at 60 °C for four hrs. The calcination occurred at the highest temperature of around 500 °C for 24 hours.

Fabrication of Fe_2O_3@SiO_2@TiO_2-Ag

The wet chemical method was used for the precipitation of Ag on Fe_2O_3@SiO_2@TiO_2surface nanocomposites was achieved by the wet chemical method (9). 3.8 g of Fe_2O_3@SiO_2@TiO_2 particles were first dissolved in 10 ml of NH_4OH and 0.5 gm of $AgNO_3$ solution for 30 min. adding 0.1 g of polyethylene glycol and 15 ml of ETOH while heating the mixture at 70 °C under a reflux process for 4 hours. The finished product was magnetically separated and then dried for 10 hours at 50 °C (13,20).

Photo-catalytic performance

A batch-mode reactor was used to degrade MTZ while being illuminated by the sun. The reactor was composed of Pyrex glass (1L) that had been coated with silver nitrate in order to prevent sunlight scattering at the bottom. In addition, a piece of the mirror was used as a refractor. Solutions of different amounts of MTZ (15, 30, 45, 50, and 80) mg/L were prepared then adjust pH, (using pH meter type INOLAB 72, WTW Co., Weilheim, Germany). Subsequently, Fe_2O_3@SiO_2@TiO_2-Ag (20, 40, and 60) mg/L was added. After that, at 200 rpm the solution was agitated using a stirrer of the MSH-300N kind (BOECO, Hamburg, Germany) in order to attain primary adsorption equilibrium before the solar photocatalyst reaction was initiated. 10 ml of the sample was taken out and centrifuged at 200 rpm for 15 minutes at regular intervals to separate the catalyst. The amount of MTZ in each sample was measured using a spectrophotometer (UV-Vis Spectrophotometer PerkinElmer 55 OSE) at a wavelength of 320 nm, then after, MTZ removal percentage was calculated by using (Eq 1).

$$\textbf{Removal eff.} = \frac{\mathbf{MTZ_o - MTZ_e}}{\mathbf{MTZ_o}} \times \mathbf{100} \quad \textbf{(1)}$$

Where MTZ_o and MTZ_erepresent both the primary and the equilibrium concentration of MTZ (mg/L), respectively.

RESULTS AND DISCUSSION

Characterization: The crystalline structures of the manufactured photocatalyst were studied using Cu Kα radiation at 2 θ and X-ray diffractometer (Bruker, D8, Germany) at 20° to 80°. Characterizing the morphologies of the synthesized photocatalyst using the scanning electron microscope (SEM) (SEM, Ultra55, ZEISS, Germany). Energy-dispersive X-ray spectroscopy (EDS) and color mapping, which are SEM-equipped, were used to look into the elemental composition. The collected samples' FTIR spectra were measured using KBr as a standard using the Nicolet 5DX-FTIR instrument. Using the Brunauer-Emmett-Teller (BET) and Barrett-Joyner-Halenda (BJH) theories, the Quantachrome SI Micromeritics apparatus was used to determine the pores diameter and specific surface area of the acquired samples. On a SHIMADZU UV-2600 spectrophotometer, the optical characteristics of manufactured catalysts were assessed. For measuring the intensity of irradiation, SOLAR POWER METER (SD Card real -time recorder Model: SPM-1116SD) was used.

UV-Vis spectroscopy

In order to study the optical properties of Fe_2O_3@SiO_2@TiO_2-Ag nanocomposite , the ultraviolet-visible diffuse reflection spectra (DRS)(UV-1800,SHIMADZU, Japan) at wavelengths ranging between 200 and 800 nm were recorded. TiO_2-Ag's absorption spectrum revealed a broad absorption of 200 nm ≤ λ ≤ 800 nm, with a peak at 610 m, as indicated in

Figure 2a. Then, Tauc's relation equation (Eq. 2) was applied to the UV-Vis measurements to calculate bandgap energy (25).

$$(\alpha h\nu)^n = A(h\nu - Eg) \qquad (2)$$

Where α is the coefficient of absorption, A is a constant with different values for different transitions, e.g., the optical energy band gap value, h is the Planks constant (6.626×10^{-34} Joules sec), hν is the light frequency, and n is a constant number that depends on the transition characteristics and can be ½, 2, 3/2 and 3 for, respectively, allowed direct, allowed indirect, forbidden direct and forbidden indirect transitions. The obtained results were then plotted using Origin Pro 8 software (Origin Lab, Northampton, MA, USA) as shown in Figure 2b. The direct optical band gap of the Fe_2O_3@SiO_2@TiO_2-Ag nanocomposite is visible at 2.51ev, which confirms the activation of biosynthesis TiO_2 in the presence of visible and solar light for application purposes (6).

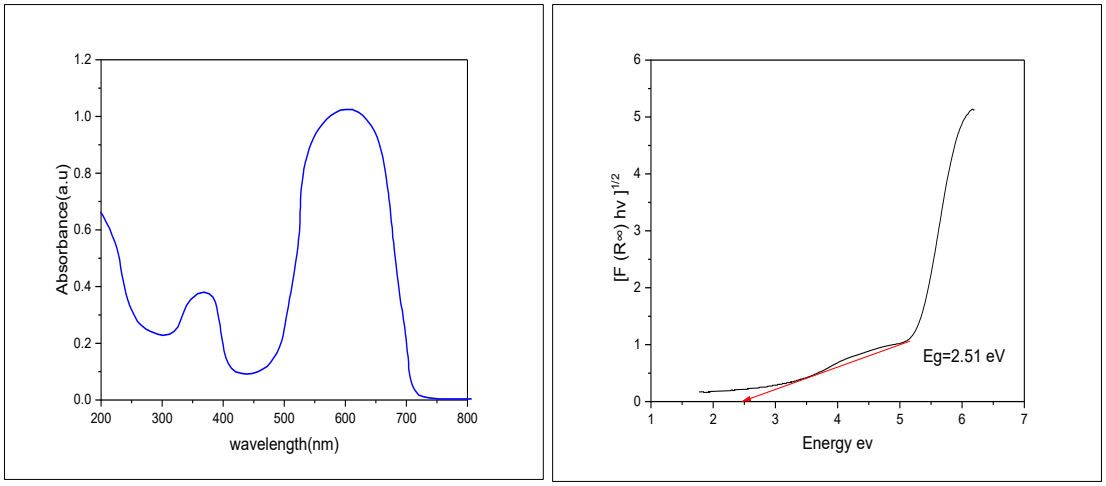

(a)Absorption spectra for nanocomposite (b) Bandgap for nanocomposite

Fig.2. UV-Vs band gap results for nanocomposite

Fourier-transform infrared spectroscopy (FTIR): The composition and structure of the nanocomposites before treatment are confirmed by the FTIR spectra of Fe_2O_3@SiO_2@TiO_2-Ag. The narrow desorption bonds at 1103.08 correspond to the asymmetric stretching vibration of Si-O-Si, likewise, stretching vibrations of O-Ti-O, O-H, Si-O-Si, and N-H were assigned to the bands between 1384.64 and 1633.41. These bands were attributed to Ti-O, Si-O-Ti stretching, and Ti-O-Ti stretching modes, as shown in Figure 3 (black line) (22). This finding demonstrated the existence of hydroxyl ions from the adsorbed water molecules on the surface of the core shale. The O-H stretch area of the hydroxyl group, which is associated to the range of (2874.38-3850.18), is where the huge peaks were observed. The stretching vibration peaks at 1055.84 cm^{-1} were formed by silica oxide (-Si-O-Si -) and (-Ti-O), respectively, as seen in Figure 3 (red line), where the peak values of O-Fe_2O_3@SiO_2@TiO_2-Agwere moved (34). A collision between the MNZ and the core shale surface is indicated by the disappearance or emergence of new bands (41). It is clear that the frequency of the various functional groupings has been altered. In other words, these organizations contributed to the MNZ response.

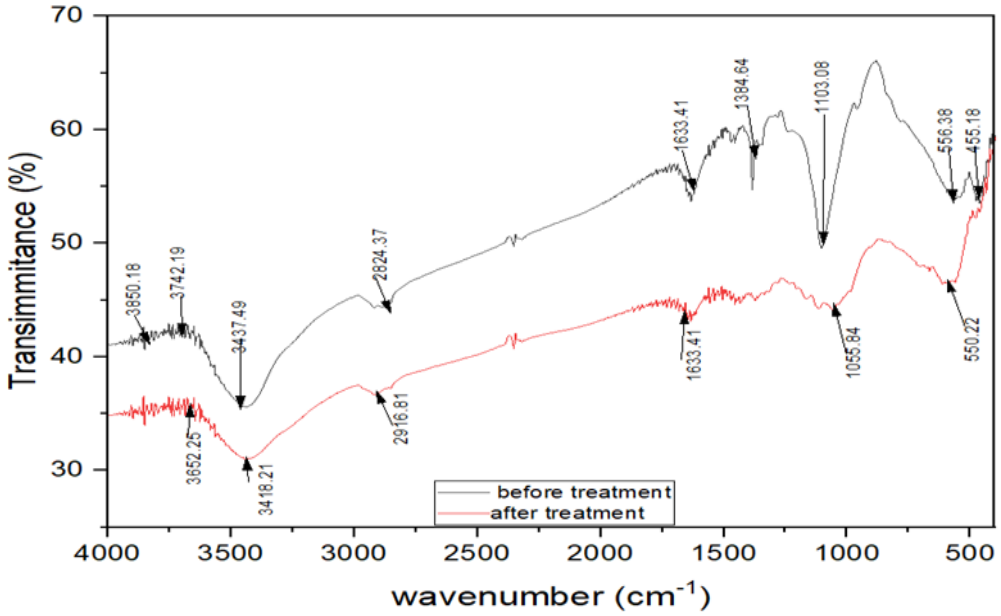

Fig.3. FTIR for nanocomposite

X-ray powder diffraction

X-ray diffraction patterns of the samples are used to analyze the phase characteristics and composition of the prepared samples. This image shows that all of the peaks are associated with the Fe_2O_3 particles (the magnetite's face-centered cubic structure), and no impurities are seen. The related peaks of Fe_2O_3 particles at 2θ of 15.511, 15.812, 18.554, 25.173, 29.333, 33.919, 39.461, 46.460, and 63.130 are (210), (221), (311), (240), (511), (420), (442), (690), and (811), respectively, which agree with the JCPDS card number 19-0629. Sharp peaks are the result of Fe_2O_3 forming with a cubic inverse spinel structure. As well, the peaks at 2θ of 25.173° (101) and 63.13° (105) confirm the presence of anatase phase (JCPDS card No. 12-2172). Whereas two peaks at 2θ=15–25 usually correspond to amorphous SiO_2. Due to the small amount of Ag particles, modest peaks of the Ag phase from the (1 1 1), (2 0 0), (2 2 0), and (3 1 1) planes of Ag NP were seen by XRD which perfectly match with the (JCPDS card No. 04-0783) (17).The physical properties of the core- Ag as well as its mean size domains calculated based on the Scherrer equation (Eq.4) (5) are present in Table 1, which shows that the crystalline size of the synthesized nanocomposite was 35.37nm.The difference in particle size can be attributed to the tendency of magnetic particles to aggregate and attract (36). $D=K\lambda/\beta\cos\theta$ (6). Where λ is the x-ray radiation wavelength (0.15418 nm),β represents the full width at half ximum (FWHM) of the diffraction peak to the suitable crystallographic plane of anatase, θ is the angle of the x-ray diffraction peak, and D is the crystallite size.

Table 1. Some physical properties of Fe_2O_3@SiO_2@TiO_2–Ag from XRD

Sample	Crystal system	Average crystallite size (nm)	d spacing (Å)	Density (g/cm^3)	FWHM
Fe_2O_3@SiO_2@TiO_2–Ag	Cubic	35.37	12	4.13	2.5

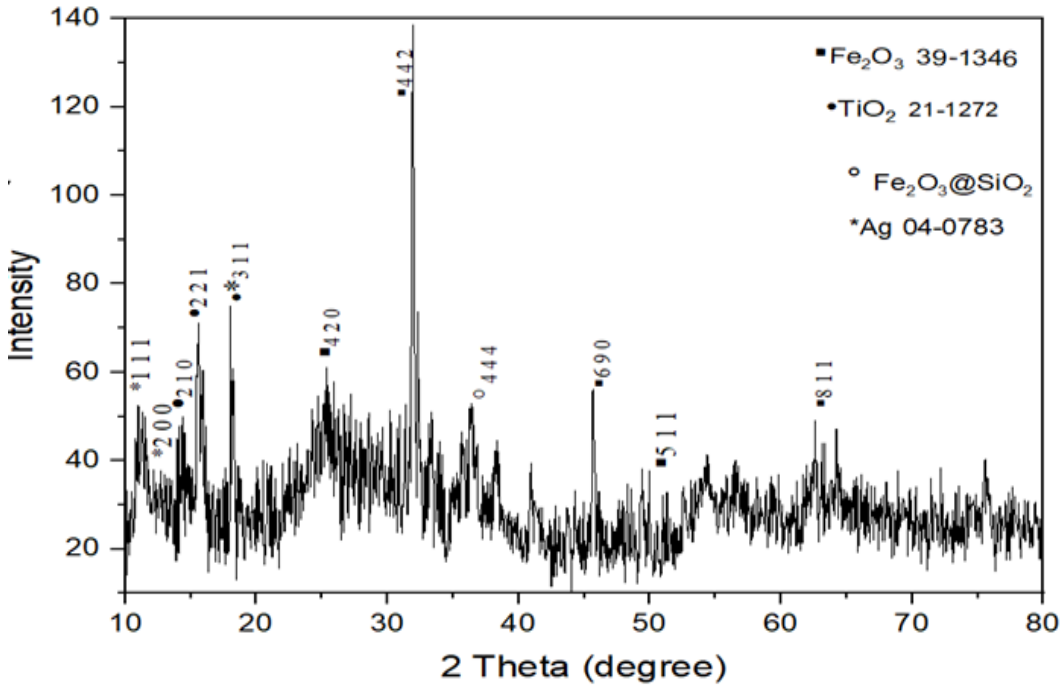

Fig.4. XRD analysis for Fe_2O_3@SiO_2@TiO_2–Ag nanocomposite

Scanning electron microscope (SEM) characterization: The morphology of Fe_2O_3@SiO_2@TiO_2–Ag nanoparticles before and after usage in the MTZ photodegradation was examined using SEM and their results are present in Figure5, the results demonstrated that the particle size of Fe_2O_3@SiO_2@TiO_2–Ag nanocomposite `ranging between (22.35-49.13) nm, whereas, after uses in MTZ, the size was reduced to around (24.56-67.76) nm. Besides that, both of them are within the nanostructures (7). As can be seen from the SEM images, the surface was rough, there were irregular spherical agglomerations, as well as numerous pores, ravines, and cracks. Actually, during the photocatalytic process, these morphological features provide a lot of surface area for sorbing impurities (23). The antibiotic molecules had penetrated the voids on the catalyst's surface, which resulted in the catalyst's surface becoming brighter and many previously separated aggregates merging. The main cause of the high rate of antibiotic removal could be attributed to this (28). EDS is an analytical method that uses X-rays released from the specimen to identify the constituent elements in a sample's chemical components or conduct an elemental analysis on it. The various elements in the sample are represented by energy peaks. Figures 5(c and d) show that the as-formed nanocomposites were entirely made up of Fe, O, Si, Ti, and Ag, confirming the deposition of TiO_2-Ag nanocrystals on the surface of the Fe_2O_3@SiO_2 nanoparticles(45).

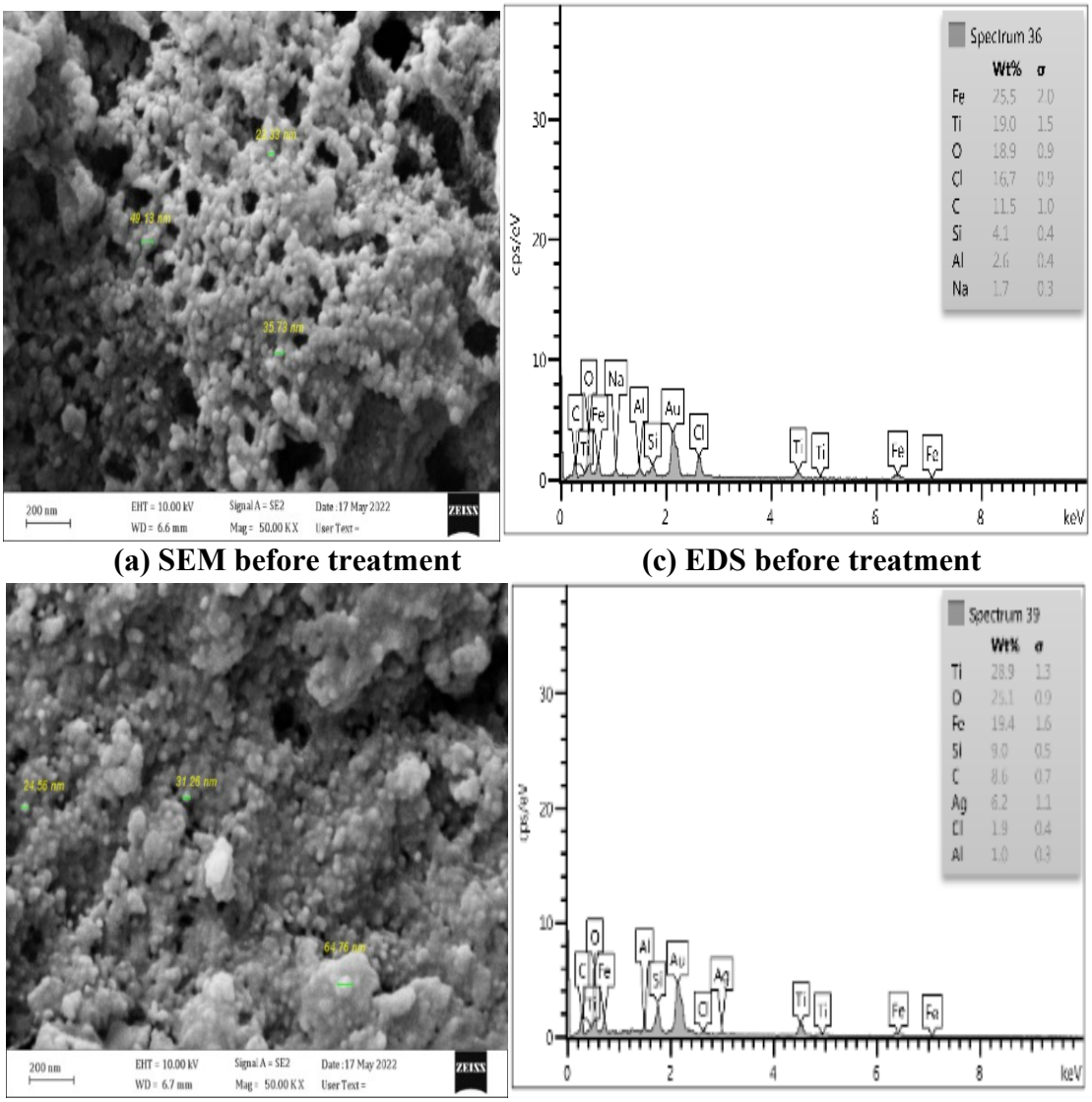

(a) SEM before treatment **(c) EDS before treatment**

(b) SEM after treatment **(d) EDS after treatment**

Fig.5. SEM-EDS of Fe_3O_4@SiO_2@TiO_2–Ag nanoparticles.

Brunauer Emmett Teller

Using the N_2 sorption isotherm, the textural properties of Fe_2O_3@SiO_2@TiO_2-Ag nanocomposite were determined. The catalyst composite displayed a type-IV isotherm with the H_3 hysteresis loop, as shown in Figure 6. The Barrett Joyner and Halden (BJH) method's specific surface area, specific pore volume, and average pore diameter (45). And their outcomes were, respectively, (58.74) m^2/g, (0.6712) cm^3/g, and 45.70 nm. The extra space made by silver nanoparticles adsorbed on the surface is to blame for this rise in the specific surface area (9

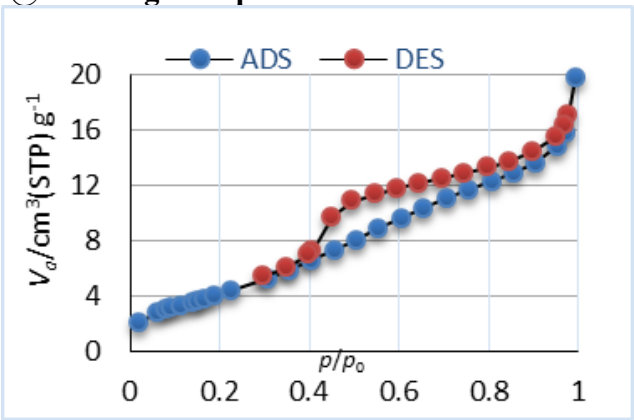

Fig.6. N_2 adsorption-desorption curves of nanocomposite

Adsorption and photocatalytic results:Comprising different processes nano-catalysts: In this study, more than one comparison was made between three types of

nano-catalyst which shows in Figure 7. The commercial traditional titanium oxide, $Fe_3O_4@SiO_2@TiO_2$, and $Fe_3O_4@SiO_2@TiO_2$–Ag was chosen and the test was done at pH=7, H_2O_2=100 mg/L, MTZ=15 mg/L, the temperature of 25°C, catalyst dosage of 25mg/L. The best one was chosen to avoid the disadvantageous effects of the other type. It was found that $Fe_3O_4@SiO_2@TiO_2$–Ag has a higher efficiency in removing MTZ, so further tests were carried out and study the different parameters that effects MTZ degradation.

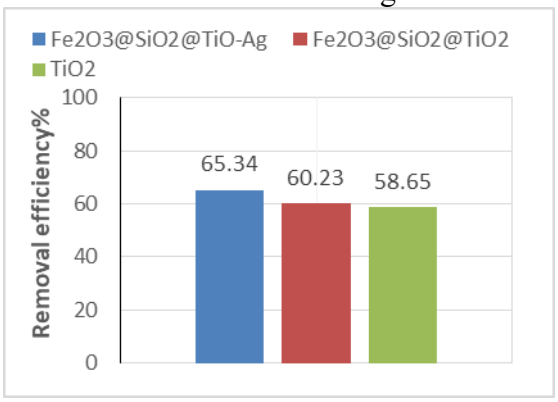

Fig.7. MTZ degradation efficiency as a function of different nano-catalysts

Influence of Ph

While maintaining other parameters (MTZ concentration of 15 mg/L, and 20 mg/L dosages of core-Ag), different pH values of 3, 5, 7, and 9 were applied. A plot of the results is shown in Figure 8, showing that MTZ removal efficiency decreased at low and high pH values as a result of the substrate and catalyst ionization, where MTZ is negatively charged at alkaline pH and positively charged at acidic pH. In contrast, the core-Ag surface charge shifts from positive to negative as a result of the core surface's electrostatic loading during photocatalytic reactions. This is due to the point zero charge for core-Ag that has been calculated at 7.25, as shown in Figure 9. Given the pH and ionic strength of the medium, core particles are demonstrated to be granules. It is known that in acidic conditions, core particle agglomeration is less dominant than under alkaline conditions (44). Increased hydroxyl radical generation at higher pH levels and antibiotic hydrolysis are the two factors responsible for the increase in degradation rate from pH 3 to pH 5. In light of this, pH 5 was the optimal removal level. The equations that follow demonstrate that under acidic and alkaline circumstances, respectively, the photocatalyst surface can become protonated and deprotonated (12).

$$pH < P_{zc}\ \ TiOH + H_2^{+} \rightarrow TiOH_2^{+} \quad (6)$$

$$pH > P_{zc}\ TiOH + OH^{-} \rightarrow TiO^{-} + H_2O \quad (7)$$

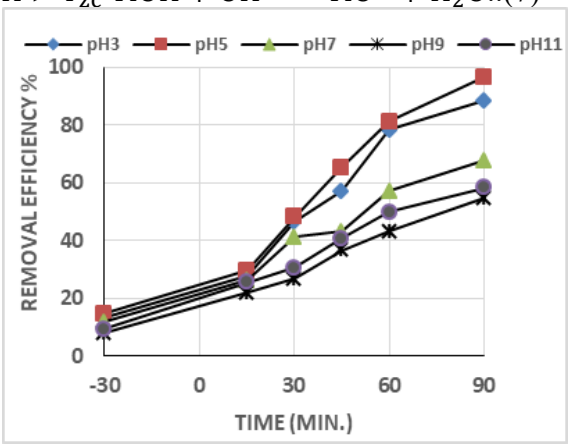

Fig.8. pH influence on the MTZ degradation

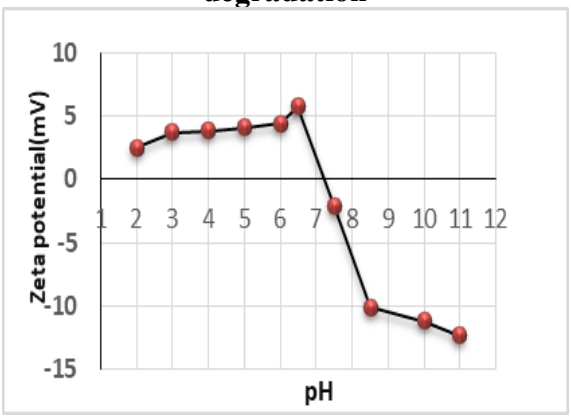

Fig.9. The point zero charge of $Fe_2O_3@SiO_2@TiO_2$-Ag

Influence of $Fe_2O_3@SiO_2@TiO_2$-Ag dosage

The amount of catalyst required to drive the photodegradation reaction has a significant impact on the photocatalytic performance against MTZ antibiotics (12). In order to test the photodegradation of 15mg/L of MTZ at a pH of 5, several dosages of as-prepared core-Ag nanocomposite (20, 40, and 60) mg/L were used. The findings are shown in Figure 10. The MTZ elimination was shown to grow from 48.32 to 96.85% by extending the illumination time from 30 to 180 min, and it achieved its maximum value at 90 minutes for a dosage of 20 mg/L of core-Ag. This effect can be explained by the fact that as photocatalyst dosage is increased, incident sunlight is blocked out more and more. Since MTZ's photocatalytic degradation decreased when its core-Ag concentration exceeded 20 mg/L. The core-Ag photocatalyst nanoparticles' aggregation on each other in the

aqueous solution, which reduces the number of sites accessible for MTZ molecule reactions, is the likely cause of the decline in MTZ removal efficiency. With 20 mg/L core-Ag, more research was conducted. Other researchers have reported outcomes that are comparable (42).

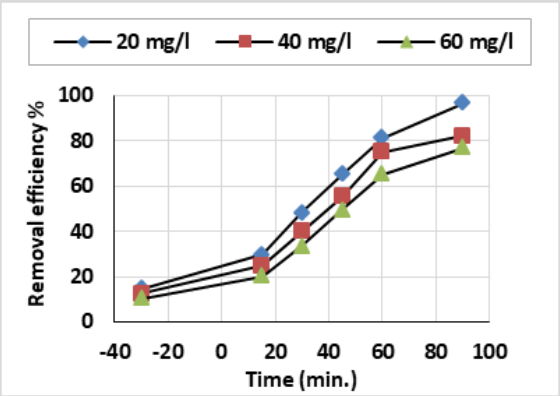

Fig.10. MTZ degradation as a function of Fe_2O_3@SiO_2 @TiO_2-Ag dosage

Influence of MTZ concentration and contact time: While maintaining other variables constant at a core-Ag amount of 20 mg/L and pH 5, the impact of the starting concentration of MTZ on the photocatalytic efficiency was examined. The findings are presented in Figure 11 and range from 15 to 80 mg/L. This graph shows that increasing the concentration of MTZ had a negative impact on removal efficiency and that after 90 minutes of solar light illumination, the degradation efficiencies of 15, 30, 45, 60, and 80 mg/L, respectively, were 96.85, 72.12, 65.17, 56.12, and 45.74%. As the antibiotic concentration rises, more antibiotic-adsorbed photocatalyst surfaces. On the surface of the catalyst, photoactive patches are diminished, and the rate of antibiotic deterioration is also diminished. Additionally, the levels of produced radicals were constant across all samples. The removal of hydroxyl radicals was more likely to occur in samples with lower concentrations of MTZ than in samples with higher concentrations of antibiotic (32,37). As antibiotic concentration increases, more antibiotics are adsorbed to the photocatalyst surface. Degradation of antibiotics occurs more slowly due to diminished photoactive patches on the catalyst surface (12).

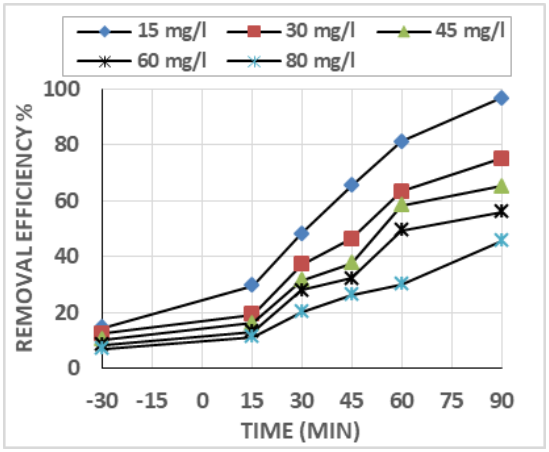

Fig.11. MTZ elimination percentage as a function of initial concentrations of MTZ.

Reusing and recycling of catalyst

The catalyst's capacity for numerous reuse in the process suggests that it may find use in industry. The Fe_2O_3@SiO_2@TiO_2-Ag catalyst's capacity to be reused was assessed in the current work throughout the course of four subsequent cycles under precisely controlled conditions. The nanocomposites were removed from the solution by a magnetic separator at the end of each run cycle, rinsed three times with deionized water, dried in an oven at 80 °C for 60 min, and then used in the following cycle. As seen in Figure 12, Fe_2O_3@/SiO_2@TiO_2-Ag's activity reduced after each reaction cycle, and after five cycles were evaluated, removal efficiency steadily fell from 96.85% (origin) to 61.12%. (cycle 4). The catalyst surface may partially leach, which results in the degeneration of the active catalytic sites, and cause this drop in activity. Another cause of the catalyst's decreased activity is the washing and drying processes' inability to completely remove the reactants and byproducts from the cavities and active sites of the catalyst. The surface of the catalyst particles may also be filled with intermediates which absorb on the surface of the core-Ag particles and fill the zones on the catalyst surface because of the intermediates available (16,43). It can be inferred that the Fe_2O_3@SiO_2@TiO_2-Ag catalyst has a high degree of stability and reusability potential. As a result, the catalyst's industrial use may have lower operating costs..

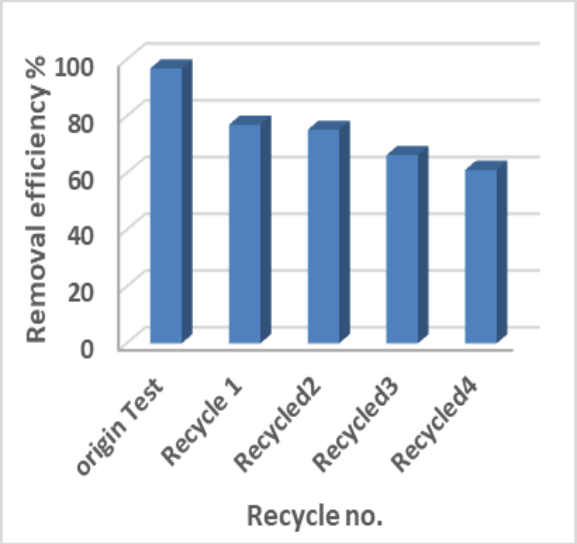

Fig.12. the relationship between removal efficiency and the recycling runs

Influence of intensity

The selection of the irradiance range in the experiment was made based on annual solar irradiance data in Iraq -Diyala (temperate, warm transitional climate). As presented in Figure 13 that increasing light intensity from (106.8 MW/cm^2) to (959.5 MW/cm^2) increases the MTZ removal from 69.7% to 96.85% from April to July. Hydroxyl radical production enhances the removal rate. A catalyst absorbs more photons when the solar power increases. This increases the number of hydroxyl radicals produced by the catalyst, thereby increasing the chances of photon activation on the catalyst surface and increasing the photocatalytic power (38). Also, it can be observed from this figure that the intensity of solar irradiance certainly fluctuated that affecting the removal rate as a result of several environmental variables and electron/hole recombination catalysts (39)

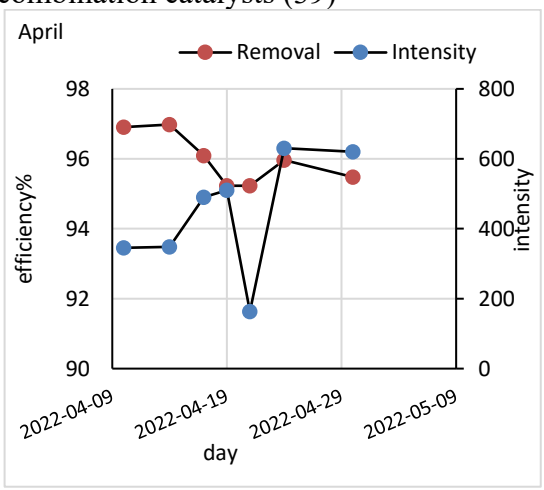

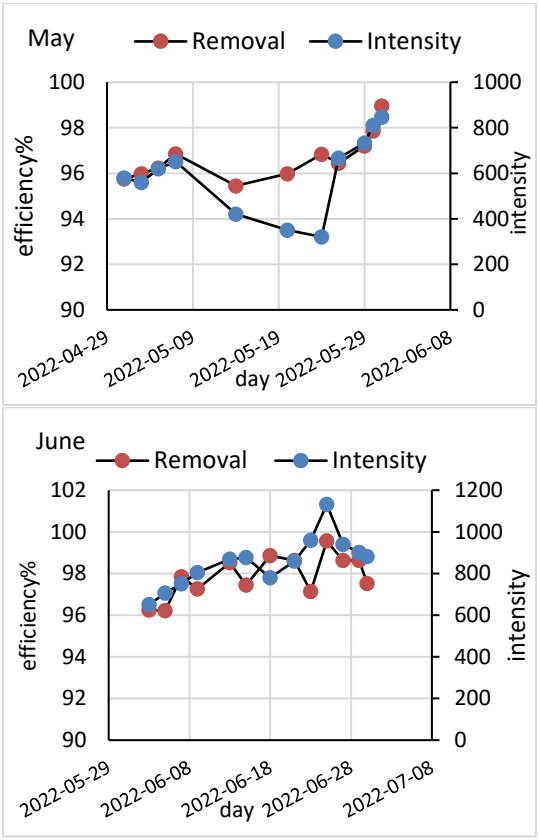

Fig.13. Effect of solar intensity on the removal efficiency

kinetic of photodegradation

The dynamic collaboration between antibiotic and core-Ag surfaces is essential for understanding the performance of the solar photocatalytic process for MTZ elimination from synthetic wastewater. Generally, pseudo-first-order kinetics is used to illustrate the reaction rate of heterogeneous catalysis, which can also be explained by Langmuir-Hinshelwood (L-H) kinetics (35,40).

$$\ln \frac{C_o}{C} = k_{obs} \cdot t \qquad (8)$$

Where: k_{obs} represent reaction rate constant (1/min), C and Co are the amounts of MTZ in mg/L following exposure time t, and the concentration at the start, respectively and t is the exposure time (min). Plotting $\ln\left(\frac{C_o}{C_t}\right)$ as a function of t from 0 to 90 minutes produces the kinetics results, as shown in Figure 14 and the values of K_{obs}, as well as the coefficient of regression (R^2) of the linear plot equations, are present in Table 2. As presented in this table increasing MTZ concentrations reduces the results for the constant degradation rate of K_{obs}. Furthermore, higher R^2 values >93, suggesting the suitability of a pseudo-first-order kinetic model for representing the use of

Fe_2O_3@SiO_2@TiO_2-Ag for MTZ photodegradation, this agrees with the experimental findings in section 3.2.2 on how the initial MTZ concentrations influence the removal efficiency.

Table 2. Reaction rate parameters for MTZ degradation

MTZ conc.	Removal eff.%	K_{obs}	R^2	Equation
15	96.85	0.033	0. 945	y = 0.0328x - 0.1624
30	75.12	0.019	0.975	y = 0.0186x - 0.0976
45	65.17	0.013	0.983	y = 0.0126x - 0.0065
60	56.12	0.009	0.981	y = 0.0091x + 0.0254
80	45.74	0.006	0.993	y = 0.0063x + 0.0173

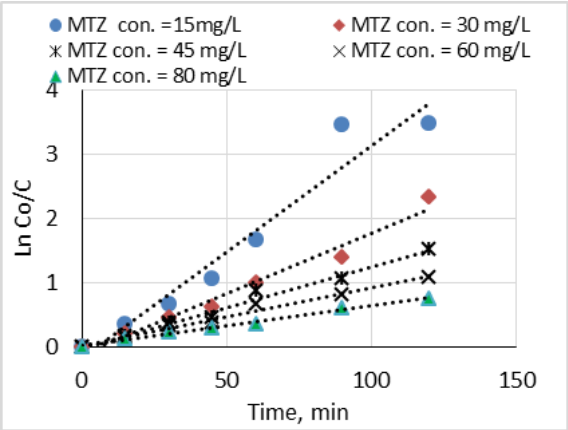

Fig.14. Kinetic curve for MTZ elimination at different initial concentrations.

CONCLUSION

The combination procedures of precipitation, sol-gel, and photo-deposition were used to fabricate Fe_2O_3@SiO_2@TiO_2-Ag magnetically separable photocatalyst. Nanoparticles that had already been synthesized were satisfactorily characterized using XRD, SEM, EDS, and FTIR methods. An environmentally benign catalyst, the Ag-doped nanocomposite, was employed to photocatalyst the breakdown of the antibiotic MTZ. By raising the catalyst dose, MTZ removal increased, and as MTZ concentration climbed, the degradation percentage dropped. The results, confirm that MTZ degradation was positively influenced by the pH of the solution, and the reaction was based on a first-order kinetic model. Following the completion of the photodegradation reaction, the catalysts could be easily separated from the resultant solution using magnetic separation. The findings show that Fe_2O_3@SiO_2@TiO_2-Ag photocatalyst is stable after recycling and exhibits potential performance as an inexpensive and ecologically acceptable method for photocatalytic treatment of wastewater.

CONFLICT OF INTEREST

The authors declare that they have no conflicts of interest.

DECLARATION OF FUND

The authors declare that they have not received a fund.

REFERENCES

1.Abbasian, R., and H. Jafarizadeh-Malmiri, 2020. Green approach in gold, silver and selenium nanoparticles using coffee bean extract. Open Agriculture, 5(1), 761–767. https://doi.org/10.1515/opag-2020-0074.

2.Abbasiasl, H., M. Mehdi, and M. Ghaedi, 2021. Journal of Environmental Chemical Engineering Efficient degradation of metronidazole antibiotic by TiO_2/Ag_3PO_4 /g – C_3 N_4 ternary composite photocatalyst in a continuous flow-loop photoreactor. Journal of Environmental Chemical Engineering, 9(5), 105963. https://doi.org/10.1016/j.jece.2021.105963.

3.Abdulmajeed, B. A., S. Hamadullah and F. A. Allawi 2019. Synthesis and characterization of titanium dioxide nanoparticles under different pH conditions. Journal of Engineering, 25(1), 40-50. https://doi.org/10.31026/j.eng.2019.01.04

4.Aboudalle, A., H. Djelal, F. Fourcade, L. Domergue, A. A. Assadi, T. Lendormi, S. Taha and A. Amrane 2018. Metronidazole removal by means of a combined system coupling an electro-Fenton process and a conventional biological treatment By-products monitoring and performance enhancement. Journal of Hazardous Materials, 359, 85-95. 10.1016/j.jhazmat.2018.07.006.

5.Alwared, A. I., F. A. Sulaiman, H. Raad, T.J. Al-Musawid and N. A. Mohammed 2023. Ability of $FeNi_3$/SiO_2/TiO_2 nanocomposite to degrade amoxicillin in wastewater samples in solar light-driven processes. South African Journal of Botany, 153, 195-202. https://doi.org/10.1016/j.sajb.2022.12.031

6.Askari, N., M. Beheshti, D. Mowla, and M. Farhadian, 2020. Synthesis of $CuWO_4$/Bi_2S_3 Z-scheme heterojunction with enhanced

cephalexin photodegr-adation. Journal of Photochemistry and Photobiology A: Chemistry, 394, 112463. https://doi.org/10.1016/j.jphotochem.2020.112463

7.Chatterjee, A., D. Nishanthini, N. Sandhiya and J. Abraham 2016. Biosynthesis of titanium dioxide nanoparticles using Vigna radiata. Asian Journal of Pharmaceutical and Clinical Research, 85–88. https://doi.org/10.22159/AJPCR.2016.V9S2.13405

8.Cheyne, R. W., T. A. Smith, L. Trembleau and A. C. Mclaughlin 2011. Synthesis and characterisation of biologically compatible TiO_2 nanoparticles. Nanoscale research letters, 6(1), 1-6. https://doi.org/10.1186/1556-276X-6-423

9.Chi, Y., Q. Yuan, Y. Li, L. Zhao, N. Li, X. Li and W. Yan 2013. Magnetically separable Fe_3O_4@ SiO_2@ TiO_2-Ag microspheres with well-designed nanostructure and enhanced photocatalytic activity. Journal of hazardous materials, 262, 404-411. https://doi.org/10.1016/j.jhazmat.2013.08.077

10.Cui, B., H. Peng, H. Xia, X. Guo and H. Guo 2013. Magnetically recoverable core–shell nanocomposites γ-Fe_2O_3@ SiO_2@ TiO_2–Ag with enhanced photocatalytic activity and antibacterial activity. Separation and Purification Technology, 103, 251-257. https://doi.org/10.1016/j.seppur.2012.10.008

11.Dabirvaziri, B., M. H. Givianrad, I. Sourinejad, A. M. Moradi and P. G. Mostafavi 2019. A simple and effective synthesis of magnetic γ-Fe_2O_3@ SiO_2@ TiO_2–Ag microspheres as a recyclable photocatalyst: dye degradation and antibacterial potential. Journal of Environmental Health Science and Engineering, 17, 949-960. doi: 10.1007/s40201-019-00410-w.

12.Du, H., N. Li, Y. Yang, Q. Li, G. Yang and Q. Wang 2023. Plasmonic Ag modified Ag_3VO_4/AgPMo S-scheme heterojunction photocatalyst for boosted Cr (VI) reduction under visible light: Performance and mechanism. Separation and Purification Technology, 304, 122204.

13.Du, H., N. Li, L. Yang, Q. Li, G. Yang, and Qi Wang, 2023. Plasmonic Ag modified Ag_3VO_4/AgPMo S-scheme heterojunction photocatalyst for boosted Cr(VI) reduction under visible light: Performance and mechanism, Separation and Purification Technology, 304, 2023,122204, https://doi.org/10.1016/j.seppur.2022.122204.

14. Fang, Y., Z. Li, B. Yang, S. Xu, X. Hu, Q. Liu and D. Lu 2014. Effect of dye structure on optical properties and photocatalytic behaviors of squaraine- sensitized TiO_2 nanocomposites. The Journal of Physical Chemistry C, 118(29), 16113-16125. https://doi.org/10.1021/jp502208.

15.Farzadkia, M., E. Bazrafshan, A. Esrafili, J. K. Yang and M. Shirzad-Siboni 2015. Photocatalytic degradation of metronidazole with illuminated TiO_2 nanoparticles. Journal of Environmental Health Science and Engineering, 13, 1-8. doi: 10.1186/s40201-015-0194-y.

16.Ganapathy, M., N. Senthilkumar, M. Vimalan, R. Jeysekaran and I. V. Potheher 2018. Studies on optical and electrical properties of green synthesized TiO_2@ Ag core-shell nanocomposite material. Materials Research Express, 5(4), 045020. doi: 10.1186/s40201-015-0194-y.

17.Ghasemi, Z., H. Younesi and A. A. Zinatizadeh 2016. Kinetics and thermodynamics of photocatalytic degradation of organic pollutants in petroleum refinery wastewater over nano-TiO_2 supported on Fe-ZSM-5. Journal of the Taiwan Institute of Chemical Engineers, 65, 357-366. https://doi.org/10.1016/j.jtice.2016.05.039

18.Ghasemy-Piranloo, F., S. Dadashian and F. Bavarsiha 2019. Fe_3O_4/SiO_2/TiO_2–Ag cubes with core/shell/shell nanostructure: synthesis, characterization and efficient photo-catalytic for phenol degradation. Journal of Materials Science: Materials in Electronics, 30(13), 12757-12768. https://doi.org/10.1007/s10854-019-01641-1.

19.Görmez, F., Ö. Görmez, B. Gözmen and D. Kalderis 2019. Degradation of chloramphenicol and metronidazole by electro-Fenton process using graphene oxide-Fe_3O_4 as heterogeneous catalyst. Journal of Environmental Chemical Engineering, 7(2), 102990. https://doi.org/10.1016/j.jece.2019.102990

20.Hasan, Y. R., M. A. A. Shaban, M. A. Ibrahim, M. J. M-Ridha and H. A. Hussein 2023. Effect of calcination temperature on the

adsorption performance of MG/AL layered double hydroxide nanoparticles in the removal of meropenem antibiotics. Iraqi Journal of Agricultural Sciences, 54(1), 42-58. https://doi.org/10.36103/ijas.v54i1.1675

21.He, M., D. Li, D. Jiang and M. Chen 2012. Magnetically separable γ-Fe_2O_3@SiO_2@Ce-doped TiO_2 core–shell nanocomposites: Fabrication and visible-light-driven photocatalytic activity. Journal of Solid State Chemistry, 192, 139-14. https://doi.org/10.1016/j.jssc.2012.04.004

22.Hu. Y., G. Wang, M. Huang, K. Lin, Y. Yi, Z. Fang, P. Li, and K. Wang. 2017. Enhanced degradation of metronidazole by heterogeneous sono-Fenton reaction coupled ultrasound using Fe_3O_4 magnetic nanoparticles. Environmental Technology,1-22. doi: 10.1080/09593330.2017.1374470. Epub ahead of print. PMID: 28857685.

23.Huang, D. G., S. J. Liao, W. B. Zhou, S. Q. Quan, L. Liu, Z. J. He and J. B. Wan 2009. Synthesis of samarium- and nitrogen-co-doped TiO_2 by modified hydrothermal method and its photocatalytic performance for the degradation of 4-chlorophenol. Journal of Physics and Chemistry of Solids, 70(5), 853–859. https://doi.org/10.1016/j.jpcs.2009.04.005

24.Joghataeian, M., A. Bahari, A. Qavami and M. J. Raeisi 2020. An antibacterial study of a new magnetic carbon nanotube/core-shell nanohybrids. Journal of Environmental Chemical Engineering, 8(5), 104150. https://doi.org/10.1016/j.jece.2020.104150

25.Kargar, F., A. Bemani, M. H. Sayadi, N. Ahmadpour 2021. Synthesis of modified beta bismuth oxide by titanium oxide and highly efficient solar photocatalytic properties on hydroxychloroquine degradation and pathways. Journal of Photochemistry and Photobiology A: Chemistry, 419, 113453. https://doi.org/10.1016/j.jphotochem.2021.113453

26.Kaur, H., S. Kaur, J. Singh, M. Rawat and S. Kumar 2019. Expanding horizon: green synthesis of TiO_2 nanoparticles using Carica papaya leaves for photocatalysis application. Materials Research Express, 6(9), 095034. DOI 10.1088/2053-1591/ab2ec5

27.Kulkarni, V., V. Palled, S. Hiregoudar, K. Prakash, D. Maski and S. Lendra 2019. Biosynthesis and characterization of titanium dioxide nanoparticles (TiO_2) using Azadirachta indica leaf (neem leaf) extract. International Journal of Current Microbiology and Applied Sciences 8, 2309-2317. https://doi.org/10.1016/j.sajb.2019.05.024

28.Li, C. J., J. N. Wang, B. Wang, J. R. Gong and Z. Lin 2012. A novel magnetically separable TiO_2/$CoFe_2O_4$ nanofiber with high photocatalytic activity under UV–vis light. Materials Research Bulletin, 47(2), 333-337. https://doi.org/10.1016/j.materresbull.2011.11.012

29.Malakootian, M., A. Nasiri and M. Amiri Gharaghani 2020. Photocatalytic degradation of ciprofloxacin antibiotic by TiO_2 nanoparticles immobilized on a glass plate. Chemical Engineering Communications, 207(1), 56-72. https://doi.org/10.1080/00986445.2019.1573168

30.Malakootian, M., N. Olama, M. Malakootian and A. Nasiri 2019. Photocatalytic degradation of metronidazole from aquatic solution by TiO_2-doped Fe^{3+} nano-photocatalyst. International journal of environmental science and technology, 16, 4275-4284. https://doi.org/10.1007/s13762-018-1836-2.

31.Marsooli, M. A., M. Rahimi-Nasrabadi, M. Fasihi-Ramandi, K. Adib, M. Eghbali-Arani, F. Ahmadi and Y. Joseph 2020. Preparation of Fe_3O_4/SiO_2/TiO_2/$CeVO_4$ nanocomposites: investigation of photocatalytic effects on organic pollutants, bacterial environments, and new potential therapeutic candidate against cancer cells. Frontiers in pharmacology, 11, 192. https:/doi: 10.3389/fphar.2020.00192. PMID: 32194419; PMCID: PMC7064640.

32.Mhemid, R.K.S., L.I. Saeed, and R.N. Mohammed, 2024 Photocatalytic removal of diazinon with Ag-coated SiO_2@TiO_2 core–shell using the response surface methodology. Int. J. Environ. Sci. Technol. **21**, 329–340. https://doi.org/10.1007/s13762-023-05134-x.

33.Mohammed, I., J. Mohammed, A. U. Kende, A. M. Wara, Y. A. Aliero, U. Z. Magawata, A. B.Umar and A. K. Srivastava, 2023. Review on Y-type hexaferrite: synthesis, characterization and properties. Applied

Surface Science Advances, 16, 100416. https://doi.org/10.1016/j.apsadv.2023.100416.

34.Mohanta, D., and M. Ahmaruzzaman, 2021. Facile fabrication of novel Fe_3O_4-SnO_2-gC_3N_4 ternary nanocomposites and their photocatalytic properties towards the degradation of carbofuran. Chemosphere, 285, 131395.
doi: 10.1016/j.chemosphere.2021.131395

35.Nabipour H., M. Hosaini Sadr and N. Thomas 2015. Synthesis, characterisation and sustained release properties of layered zinc hydroxide intercalated with amoxicillin trihydrate. Journal of Experimental Nanoscience, 10(16), 1269–1284.
https://doi.org/10.1080/17458080.2014.998301

36.Nasseh, N., L. Taghavi, B. Barikbin and M. A. Nasseri 2018. Synthesis and characterizations of a novel $FeNi_3/SiO_2/CuS$ magnetic nanocomposite for photocatalytic degradation of tetracycline in simulated wastewater. Journal of Cleaner Production, 179, 42-54.
https://doi.org/10.1016/j.jclepro.2018.01.052

37.Nasseh, N., L. Taghavi, B. Barikbin, M. A. Nasseri and A. Allahresani 2019. $FeNi_3/SiO_2$ magnetic nanocomposite as an efficient and recyclable heterogeneous fenton-like catalyst for the oxidation of metronidazole in neutral environments: Adsorption and degradation studies. Composites Part B: Engineering, 166, 328-340.
https://doi.org/10.1016/j.compositesb.2018.11.112.

38. Olama N., M. Dehghani and M. Malakootian 2018. The removal of amoxicillin from aquatic solutions using the TiO_2/UV-C nanophotocatalytic method doped with trivalent iron. Applied Water Science, 8, 1–12. https://doi.org/10.1007/s13201-018-0733-7

39.Oliveira, A., E. M. Saggioro, T. Pavesi, J. C. Moreira and L. F. V. Ferreira 2012. Solar photo-chemistry for environmental remediation-advanced oxidation processes for industrial wastewater treatment. Molecular Photochemistry-Various Aspects. Rijeka: InTech, 195-223.
http://dx.doi.org/10.5772/38444.

40.Rasheed, H. U., X. Lv, W. Wei, D. K. Sam, N.Ullah, J.Xie, & Zhu, W. (2019). Highly efficient photocatalytic degradation of the Tetracycline hydrochloride on the α-Fe2O3@CN composite under the visible light. Journal of Environmental Chemical Engineering, 7(5).
https://doi.org/10.1016/j.jece.2019.103322

41.Rastkari, N., A. Eslami, S. Nasseri, E. Piroti and A. Asadi 2017. Optimizing parameters on nanophotocatalytic degradation of Ibuprofen using UVC/ZnO processes by response surface methodology. Polish Journal of Environmental Studies, 26(3).
https://doi.org/10.15244/pjoes/64931.

42.Safni, S., M. R. Wahyuni, K. Khoiriah and Y. Yusuf 2019. Degradation of Phenol by photolysis using N-doped TiO_2 catalyst. Molekul, 14(1), 6-10.
https://doi.10.20884/1.jm.2019.14.1.447.

43.Seidmohammadi, A., Y. Vaziri, A. Dargahi and H. Z. Nasab 2021. Improved degradation of metronidazole in a heterogeneous Photo-Fenton oxidation system with PAC/Fe_3O_4 magnetic catalyst: biodegradability, catalyst specifications, process optimization, and degradation pathway. Biomass Conversion and Biorefinery, 1-17.
https://doi.org/10.1007/s13399-021-01668-7

44.Shylesh, S., L. Wang and W. R. Thiel 2010. Palladium (II)-Phosphine complexes supported on magnetic nanoparticles: filtration-free, recyclable catalysts for suzuki–miyaura cross-coupling reactions. Advanced Synthesis and Catalysis, 352(2-3), 425-432.
https://doi.org/10.1002/adsc.200900698

45.Sulaiman F. A., R. K. S. Mhemid, and N. A. Mohammed 2025. Enhanced 4-chlorophenol adsorption from aqueous solution using eco-friendly nanocomposite. Ecological Engineering and Environmental Technology. 26(5), 174–189.
https://doi.org/10.12912/27197050/203126.

46.Sutrisno H., E. D. Siswani and K. S. Budiasih 2018. The effect of sintering temperatures of TiO_2 (B)-nanotubes on its microstructure. Science of Sintering, 50(3), 291-298.
https://doi.org/10.2298/SOS1803291S

47.Xue, C., Q. Zhang, J. Li, X. Chou, W. Zhang, H. Ye and P. J. Dobson 2013. High photocatalytic activity of Fe_3O_4-SiO_2-TiO_2 functional particles with core-shell structure. Journal of Nanomaterials, 2-2.
https://doi.org/10.1155/2013/762423